# Experimental and theoretical studies of the factors that influence the determination of molybdenum by electrothermal atomic absorption spectroscopy

**ARTICLE** *in* ANALYTICAL CHEMISTRY · APRIL 1993

Impact Factor: 5.64 · DOI: 10.1021/ac00056a027



**4 AUTHORS**, INCLUDING:

Pedro Araujo
National Institute of Nutrition and Seafood R…
**54** PUBLICATIONS **791** CITATIONS
SEE PROFILE

Anibal Sierraalta
Venezuelan Institute for Scientific Research
**94** PUBLICATIONS **795** CITATIONS
SEE PROFILE

Fernando Ruette
Venezuelan Institute for Scientific Research
**122** PUBLICATIONS **1,042** CITATIONS
SEE PROFILE

# Experimental and Theoretical Studies of the Factors That Influence the Determination of Molybdenum by Electrothermal Atomic Absorption Spectroscopy

**Zully Benzo,*,† Pedro Araujo,† Anibal Sierraalta,‡ and Fernando Ruette*,‡**

*Laboratorio de Química Analítica, Laboratorio de Química Computacional, Centro de Química, IVIC, Apartado Postal 21827, Caracas 1020-A, Venezuela*

**The effect of mineral acids on Mo electrothermal atomization atomic absorption signal (eaaas) was analyzed by the response surface method and by modeling Mo–graphite interactions using quantum mechanical calculations. A multivariate optimization approach was carried out using the Doehlert matrix and a cubic equation to approximate the experimental response. The results show that HCl and $HNO_3$ acids produce an enhancement of the Mo aa signal with respect to the nonacidified solution. This enhancement is interpreted as a decrease of memory effects caused by the acid presence which facilitates formation of Mo species that can be more easily atomized. Qualitative theoretical calculations (CNDO) reveal that the adsorption of Mo and $MoO_3$ occurs on 6-fold center sites. Protons coadsorbed on the graphite surface facilitate the migration of Mo species.**

## INTRODUCTION

Molybdenum is a microelement of great interest, which has been found to be an essential trace element in man[1] and an important micronutrient for plants and animals. The level of this metal, usually found in different type of samples, is so low that its determination by most analytical techniques is difficult.

Atomic absorption spectroscopy with electrothermal atomization (eaaas), owing to its high sensitivity, is one of the most widely used techniques for the trace metal determination in an ample variety of samples. The use of electrothermal atomization aas for determining trace amounts of molybdenum is, therefore, of analytical importance.

Due to the fact that molybdenum can form highly thermally stable carbides,[2-8] it must be run at the maximum temperature attainable. At this high temperature, the coating of the graphite surface gets used up, causing a reduction in its performance characteristics. Thus, repeated recalibration has to be carried out after running the samples. Tube life is shortened under these conditions and carryover between injections is often a problem.

Interference effects for Mo determination by eaas have been investigated by several authors.[2,3,6,9-14] Rather ambiguous results have been reported concerning interference effects by mineral acids; see Table I. The forms of dependence of the Mo aa signal on the ashing temperature also differ according to the work of different authors.[3,4,7,15,16]

It is clear that the interference effect of mineral acids has not been elucidated yet, as well as the dependence of the Mo analytical signal on the ashing temperature. In this work, a series of experiments were carried out, in order to determine the effect of HCl and $HNO_3$ on the molybdenum sensitivity. In addition, a multivariate study was performed using the response surface methodology for the purpose of understanding the effect of HCl concentration, ashing temperature, and atomization temperature on the Mo eaaas signal.

Theoretical methods based on quantum chemistry have been extensively employed to study surface processes.[20] The atomization of samples on graphite furnaces can be considered as a surface process that involves, among others, the desorption of chemisorbed atoms on the furnace surface. The complete neglect differential overlap (CNDO) method[21] has been successfully employed in modeling surface reactions, chemisorption, and dissociation mechanisms on metallic surfaces.[22-24]

Qualitative quantum chemistry calculations using the CNDO method were also performed here, in order to model the attachment of Mo and $MoO_3$ species on a furnace graphite surface. The effect of mineral acids was analyzed by considering the coadsorption of protons ($H^+$) on the graphite surface.

* To whom correspondence should be addressed.
† Laboratorio de Química Analítica.
‡ Laboratorio de Química Computacional.

(1) Morrison, G. H. Elemental Trace Analysis of Biological Materials. *CRC Crit. Rev. Anal. Chem.* **1979**, *8*, 287–320.
(2) Scott, P. E.; Michael, L. Mc.; Jaselskis, B. *Talanta* **1987**, *34*, 271–276.
(3) Volynskii, A. B.; Sedykh, E. M. *J. Anal. Chem. USSR (Engl. Transl.)* **1987**, *42*, 844–847.
(4) Schweizer, V. B. *At. Absorpt. Newsl.* **1975**, *14*, 137–141.
(5) Muller-Vogt, G.; Wendl, W.; Pfundstein, P. *Fresenius' Z. Anal. Chem.* **1983**, *314*, 638–641.
(6) Hoenig, M.; Van Elsen, Y.; Van Cauter, R. *Anal. Chem.* **1986**, *58*, 777–780.
(7) Nakahara, T.; Chakrabarti, C. L. *Anal. Chim. Acta* **1979**, *104*, 99–111.
(8) Wan Ngah, L. S.; Sarkissian, L. L.; Tyson, J. F. *Anal. Proc.* **1983**, *20*, 597–599.
(9) Studnicki, M. *Anal. Chem.* **1979**, *51*, 1336–1338.
(10) Neuman, D. R.; Munshower, F. F. *Anal. Chim. Acta* **1981**, *123*, 325–328.
(11) Baucells, M.; Lacort, G.; Roura, M. *Analyst* **1985**, *110*, 1423–1429.
(12) Jasim, F.; Awad, N. A. N.; Al-Rawi, A. T. *Microchem. J.* **1988**, *38*, 337–342.
(13) Volynskii, A. B.; Spivakov, B. Y.; Zolotov, Y. A. *J. Anal. Chem. USSR (Engl. Transl.)* **1987**, *42*, 1454–1459.
(14) Barbooti, M. M.; Jasim, F. *Talanta* **1981**, *28*, 359–364.
(15) Gohda, S.; Yamazaki, H.; Kataoka, H. *Bunseki Kagaku* **1984**, *33*, 407–412.
(16) Wu, S.; Chakrabarti, C. L.; Marcantonio, F.; Headrick, K. L. *Spectrochim. Acta* **1986**, *41B*, 651–667.
(17) Chakrabarti, C. L.; Sturgeon, R. E. *Prog. Anal. At. Spectrosc.* **1978**, *1*, 119–120.
(18) Sneddon, J.; Ottaway, J. M.; Rowston, W. B. *Analyst* **1978**, *103*, 776–779.
(19) Doehlert, D. H. *Appl. Stat.* **1970**, *19*, 231–239.
(20) (a) Simonetta, M.; Gavezzotti, A. *Adv. Quantum Chem.* **1980**, 103–158. (b) Hoffman, R. *Rev. Mod. Phys.* **1980**, *60*, 601–628. (c) Ruette, F.; Sierraalta, A.; Hernandez, A. *Quantum Chemistry Approaches to Chemisorption and Heterogeneous Catalysis*, 1st ed.; Kluwer Academic Publishers, Dordrecht, The Netherlands, 1992; pp 251–359.
(21) Pople, J. A.; Beveridge, D. L. *Approximate Molecular Orbital Theory*; McGraw-Hill: New York, 1970.
(22) Ruette, F.; Ludeña, E. V. *J. Catal.* **1981**, *67*, 266–281.
(23) (a) Hernandez, A.; Ruette, F.; Ludeña, E. V. *J. Mol. Catal.* **1987**, *39*, 21–41. (b) Castejon, H.; Hernandez, A.; Ruette, F. *J. Phys. Chem.* **1988**, *92*, 4970–4973.
(24) Ruette, F.; Valencia, N.; Sanchez-Delgado, R. *J. Am. Chem. Soc.* **1989**, *111*, 40–46.

0003-2700/93/0365-1107$04.00/0 

**Table I. Effect of Hydrochloric and Nitric Acid on the Molybdenum Absorption Signal**

| acid | acid concn (% v/v) | Mo mass (ng) | ashing temp (°C) | atomization temp (°C) | reading mode[a] | acid effect[b] | ref[c] |
|---|---|---|---|---|---|---|---|
| HCl | 0.0001–0.1 | 3.5 | 1000 | 3500 | PH | + | 9 |
| | <0.0001 | | | | | | |
| | 3.17–31.7 | 1 | | | PH | – | 14 |
| | 1.59 | 1.2 | 1200 | 2650 | | – | 13 |
| | 0–10 | 0.75 | 600 | 2800 | PA | + | * |
| $HNO_3$ | 0.0001–0.1 | 3.5 | 1000 | 3500 | PH | – | 9 |
| | <0.0001 | | | | | | |
| | 0.225–22.5 | 1 | | | PH | = | 14 |
| | 0.315–6.3 | 1 | 700 | 2750 | PH | + | 10 |
| | 10 | 0.5 | 500 | 2400 | PH | – | 11 |
| | 6 | 0.2 | 1500 | 2700 | PH/PA | – | 6 |
| | 0–10 | 0.75 | 600 | 2800 | PA | + | * |

[a] PH = peak height. PA = peak area. [b] + = enhancement. – = suppression. = = no effect. [c] * = this work.

**Table II. Instrumental Parameters**

wavelength: 313.3 nm
slit width: 0.5 nm
lamp current: 5 mA
calibration mode: peak area

| step | 1 | 2 | 3 | 4 | 5 | 6 | 7 | 8 | 9 | 10 | 11 |
|---|---|---|---|---|---|---|---|---|---|---|---|
| temp (°C) | 75 | 90 | 120 | 1700 | 1700 | 1700 | 2850 | 2850 | 2900 | 2900 | 40 |
| time (s) | 5 | 30 | 10 | 10 | 5 | 2 | 1.5 | 10 | 1 | 2 | 13 |
| argon flow rate (mL/min) | 3 | 3 | 3 | 3 | 3 | 0 | 0 | 0 | 3 | 3 | 3 |

read: steps 6–8

## EXPERIMENTAL SECTION

**Apparatus.** A Varian Techtron Model 875 atomic absorption spectrometer and a Varian GTA-95 graphite furnace were used. The spectrometer was equipped with deuterium-arc background corrector. Samples were introduced to the furnace with a GTA-95 sample dispenser. New pyrolytic graphite-coated tubes were employed. A Varian Mo hollow-cathode lamp was utilized at the 313.3-nm resonance line with a 0.5-nm spectral slit width. Argon served as the purge gas. The internal gas interrupt mode was employed during atomization. The monitor on the GTA-95 programmer unit was used to study the absorbance profiles. Peak area was taken as the reading mode. The furnace program employed is given in Table II.

Theoretical quantum chemistry calculations were carried out in a SUN-Sparc/1 workstation, the multivariate optimization approach was performed in an AcerPower 386SX personal computer.

**Reagents.** An Aldrich stock solution of Mo, 1000 μg/mL in water, and hydrochloric and nitric acids from Merck suprapure grade were used. Ultrapure water was obtained from a Milli-Q water system (Millipore Corp.). All test solutions were prepared immediately prior to use. High-purity (99.95%) argon was utilized to sheathe the graphite tube.

**Procedure.** Solutions of 50 ng/mL of Mo were used to optimize the furnace heating conditions.

Estimation of the optimal acid concentration and ashing and atomization temperatures was carried out by using a Doehlert experimetal matrix.[19]

Calculations of Mo–graphite interactions were performed by the CNDO approach[21] at the unrestricted Hartree–Fock (UHF) level. Details about parameters and modifications performed on this method are given elsewhere.[21–24] The pyrocoating tube surface was modeled by a seven-ring polycyclic aromatic system (coronene) which has been successfully used in simulating graphite surfaces.[25,26] This surface model is shown in Figure 1.

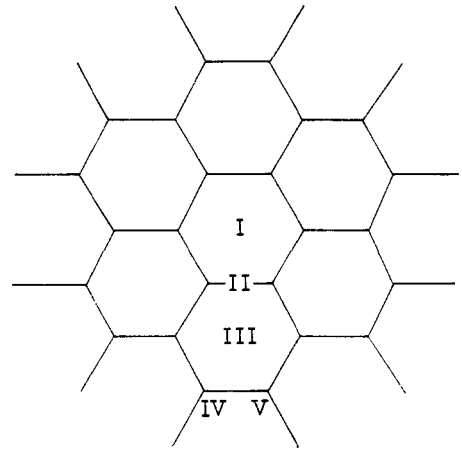


**Figure 1.** Graphite surface model.

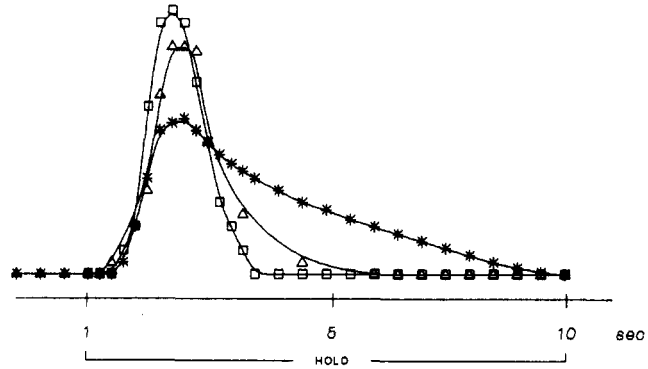


**Figure 2.** Variation of atomization profiles after 5 (□), 53 (△), and 103 (*) firings.

## RESULTS AND DISCUSSION

**Acid Effect on Mo aa Signal.** In order to understand the acid effect on the Mo aa signal, preliminary experiments were performed with acidified Mo aqueous solution, injected into the graphite furnace, under the heating conditions specified in Table 2. The signal measurements were taken by considering the integrated absorbance. This reading mode was selected after examining the Mo aa signal at different firings, shown in Figure 2. Here, it is clear that the peak height does not reproduce the Mo absorbance because a peak tail appears, whereas the peak area displays a high reproducibility. Similar observations have been reported by other authors.[17]

Our experiments have revealed that the injection of acidified Mo aqueous solution (50 ng/mL in 10% HCl) produces an enhancement (ca. 70%) of the Mo aa signal with respect to the nonacidified solution; see Figure 3. Similar results with nitric acid were observed.

A summary of the previous work, discussed in the introductory section, is presented in Table I. Here, acid concentration, Mo mass, ashing and atomization temperatures, reading mode, and acid effect are tabulated in order to compare with our results, also presented in this table. The results of this work using nitric acid compare well with Neuman's findings,[10] which have similar measurement conditions. Nevertheless, Studnicki[9] has found the same effect using HCl at quite different conditions. This is a clear indication that a variety of factors are involved in these phenomena. In view of the discrepancy between different authors regarding the acid concentration and the measurement conditions, it is difficult to reach a conclusion on the

(25) Mendoza, C.; Ruette, F. *Catal. Lett.* **1989**, *3*, 89–98.

(26) Sierraalta, A.; Benzo, de Z.; Araujo, W.; Ruette, F. *J. Mol. Struct.* **1992**, *254*, 387–393.

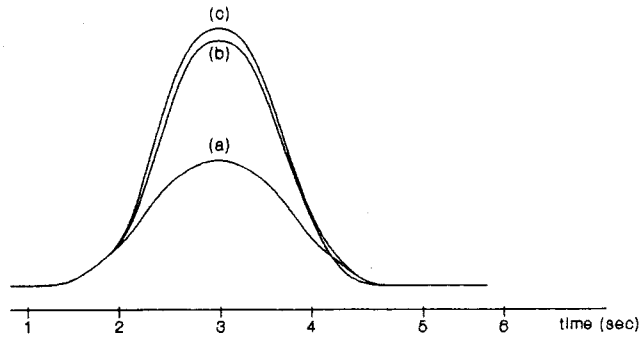


**Figure 3.** Atomization profiles: (a) Mo aqueous solution (50 ng/mL), (b) Mo acidified solution (50 ng/mL in 10% v/v of $HNO_3$), (c) Mo acidified solution (50 ng/mL in 10% v/v of HCl). Peak area: (a) 0.143, (b) 0.237, and (c) 0.243.

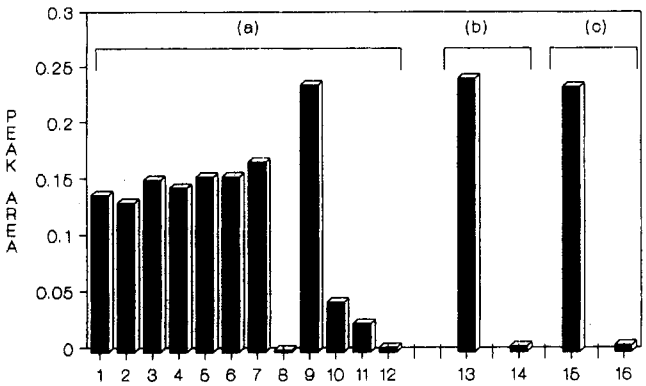


**Figure 4.** (a) Effect of HCl (10% v/v) on the removal of Mo (50 ng/mL) from the pyrolitic graphite tube. (b) and (c) decrease of the memory effect by the injection of Mo with HCl and $HNO_3$, respectively. Key: (1–7) Mo aqueous solution; (8) aqueous blank; (9–12) HCl solution; (13) Mo + HCl solution; (14) HCl blank; (15) Mo + $HNO_3$ solution; (16) $HNO_3$.

effect of mineral acids. Therefore, it is necessary to consider here a systematic study that analyzes the interactions between molybdenum, acid, and the graphite surface.

One of the features that has to be analyzed in the signal enhancement due to mineral acids is the memory effect observed in refractory carbides.[5,16–18] Figure 4a shows the results of a series of experiments, where a nonsignificant signal was observed when an aqueous blank solution was injected immediately, after successive atomizations of Mo aqueous solutions (50 mg/mL). On the other hand, a subsequent injection of HCl (10% v/v) produces a signal of approximately 1.5 times the average of those initially obtained. Subsequent injections of HCl solutions produced analytical signals whose magnitudes rapidly decrease until the baseline is reached again. These experimental results clearly reveal that in nonacidified aqueous solutions the Mo is retained on the graphite surface, although a high atomization temperature and pyrocoating tubes were used. It has been reported[3] that this tube prevents the diffusion of Mo species into the graphite body.

The above results seem to indicate that the enhancement of the Mo signal is due to the presence of mineral acids, which remove the Mo retained in the graphite tube; this in turn leads to a decrease of the observed memory effects. In order to assure that acids indeed avoid the retention of molybdenum on the graphite surface, acidified molybdenum solutions (HCl and $HNO_3$) were injected, followed by the injection of blank solutions (Figure 4b,c). The fact that the blank signals were negligible indicates that both HCl and $HNO_3$ inhibit the retention of some Mo species on the surface or in the bulk graphite. Thus, these results seem to indicate that the memory effects pointed out above are not of major concern in the presence of acids.

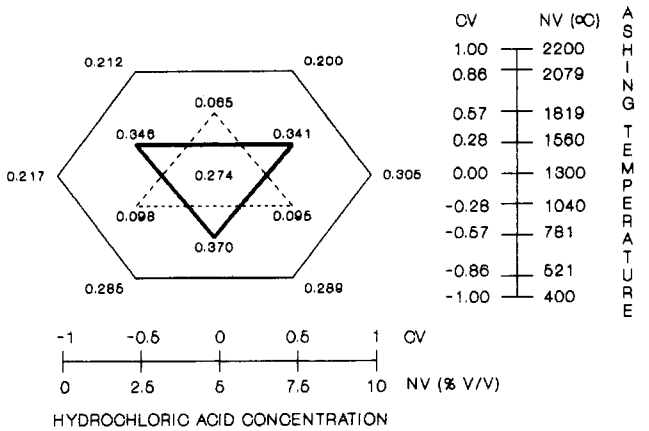


**Figure 5.** Experimental results for the experimental Doehlert matrix. For the HCl concentration and ashing temperature, two scales are shown which correspond to coded (CV) and natural (NV) variables. Atomization temperatures used: (light —) 2763 °C, (bold —) 2600 °C, and (- - -) 2437 °C.

**Table III. Experimental Field for a Doehlert Matrix: Coded Variables and the Molybdenum Measurements**

| | coded variable[a] | | | response (absorbance) | |
|---|---|---|---|---|---|
| no. | $X_1$ (0–10% v/v) | $X_2$ (400–2200 °C) | $X_3$ (2400–2800 °C) | | |
| 1 | 0 | 0 | 0 | 0.266 | 0.269 |
| | | | | 0.286 | 0.287 |
| | | | | 0.282 | 0.272 |
| | | | | 0.271 | 0.261 |
| 2 | −1 | 0 | 0 | 0.221 | 0.213 |
| 3 | −0.5 | −0.866 | 0 | 0.288 | 0.282 |
| 4 | −0.5 | −0.289 | −0.816 | 0.098 | 0.098 |
| 5 | 1 | 0 | 0 | 0.301 | 0.309 |
| 6 | 0.5 | 0.866 | 0 | 0.201 | 0.199 |
| 7 | 0.5 | 0.289 | 0.816 | 0.340 | 0.342 |
| 8 | −0.5 | 0.866 | 0 | 0.210 | 0.214 |
| 9 | −0.5 | 0.289 | 0.816 | 0.343 | 0.349 |
| 10 | 0 | −0.577 | 0.816 | 0.370 | 0.370 |
| 11 | 0.5 | −0.866 | 0 | 0.285 | 0.293 |
| 12 | 0.5 | −0.289 | −0.816 | 0.094 | 0.095 |
| 13 | 0 | 0.577 | −0.816 | 0.063 | 0.067 |

[a] $X_1$ = acid concentration. $X_2$ = ashing temperature. $X_3$ = atomization temperature.

**Multivariable Optimization Approach.** In view that there are many factors that affect the Mo signal in the presence of mineral acids, as shown in the last section, a multiple optimization approach was carried out. This technique presents several advantages: (a) Valuable information is obtained with a reduced number of experiments, compared to the classical method of optimization by one factor at a time. (b) The experimental response is studied as a function of several variables and therefore mathematically models this response. (c) Because the number of required experiments is small, the use of this technique avoids a considerable degradation of the graphite surface, due to extreme heating and acid conditions. (d) It is possible by means of this approach to obtain information regarding the interaction between the factors under study.

The variables used in this multivariate optimization were acid concentration ($X_1$), ashing temperature ($X_2$), and atomization temperature ($X_3$). In order to have a forecast of high quality, we apply the experimental matrix proposed by Doehlert.[19] The distribution of the experimental points for these three variables is given in the Figure 5, together with their natural and coded scales. The 13 experiments dictated by the Doehlert matrix are presented in detail in Table III. The acid concentration, ashing temperature, and atomization temperature were varied between 0 and 10% v/v, 400 and

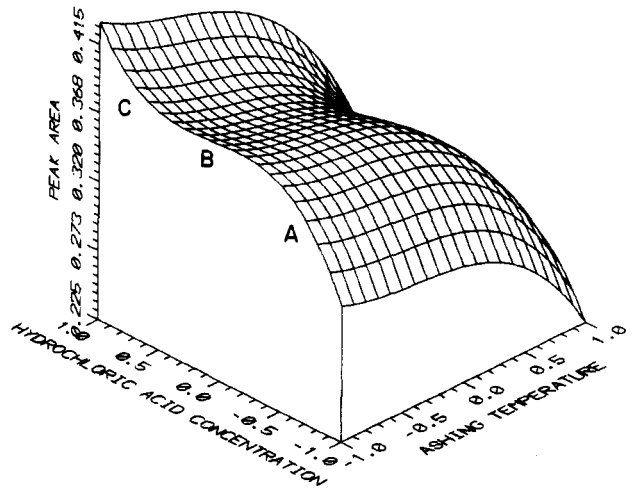


**Figure 6.** Surface response for ashing temperature and HCl concentration at the atomization temperature of 2800 °C.

2200 °C, and 2400 and 2800 °C, respectively. All the points, shown in Figure 5, represent the average of two measurements, except the central point which is the average of eight runs measured among experiments, in order to control any tube baseline drift.

The results of this study (Table III) show that the experimental response, as a function of the coded variables levels, can be approximated by a cubic equation: $Y_{Mo} = 0.274 - 0.020X_1 - 0.027X_2 + 0.161X_3 - 0.013X_1^2 - 0.033X_2^2 - 0.071X_3^2 - 0.009X_1X_2 + 0.002X_1X_3 - 0.003X_2X_3 + 0.064X_1^3 - 0.027X_2^3 + 0.000X_3^3 - 0.001X_1X_2X_3$ (1) where $Y_{Mo}$ represents the absorbance of Mo in peak area and $X_1$, $X_2$, and $X_3$ are the coded variables described above. One can conclude from the magnitude of the coefficients in this equation that the interaction between the variables is small (0.009, 0.002, 0.003, and 0.001 for $X_1X_2$, $X_1X_3$, $X_2X_3$, and $X_1X_2X_3$, respectively). Therefore, terms that contain the interaction between variables would be important only at high values of the correspondent variables.

Figure 5 shows the experimental responses obtained by the simultaneous variation of the acid concentration, ashing temperature, and atomization temperature, at each point of the Doehlert matrix. It can be seen from this figure that best responses are obtained with the highest atomization temperature (ca. 2800 °C). This result was expected since refractory elements, such as Mo, must be run, at high atomization temperatures in order to be totally atomized.

The response surface obtained from eq 1, using as variables the HCl concentration and the ashing temperature at the optimum atomization temperature (2800 °C), is plotted in Figure 6. It can be seen from this figure that an increase in the acid concentration produces, in general, an enhancement of the Mo signal in the range of ashing temperatures 400–1300 °C. Nevertheless, the change of the signal (slope) is not constant as the acid concentration increases. There is a region around 5% v/v in which the signal slightly changes. The magnitude of the signal at ashing temperatures above of 1300 °C is also affected by the loss of Mo species due to volatilization. This feature is consistent with the results reported by other authors[7,16] in which a drop in the Mo aa signal has been reported at about 1200 °C.

On the basis of these results one can select an optimal experimental field in the region of 2–8% v/v HCl and 400–1030 °C ashing temperautre (−0.6 to +0.6 and −1.0 to −0.3 in coded variables, respectively). It is advisable to use diluted acid solutions (ca. 2% v/v) to avoid the destruction of the pyrolytic graphite layer and low ashing temperatures to preclude the loss of Mo due to volatilization.

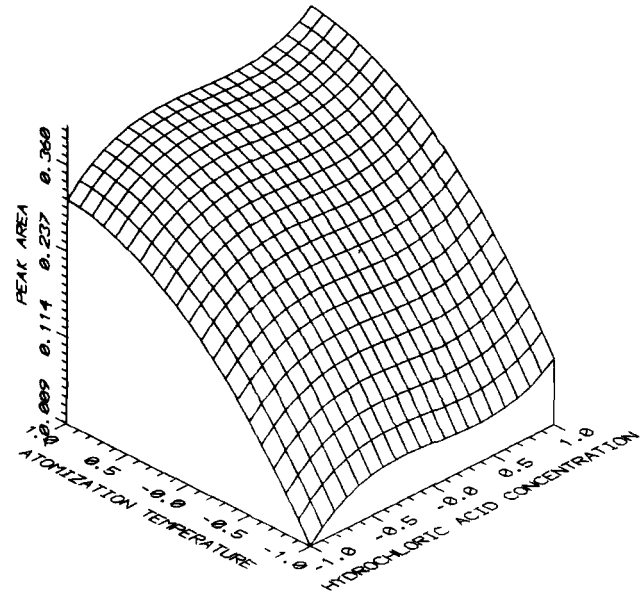


**Figure 7.** Surface response for atomization temperature and HCl concentration at the ashing temperature of 700 °C.

The response surface for atomization temperature and acid concentration at an ashing temperature of about 700 °C (−0.66 in coded variables) is plotted in Figure 7. The results show a similar behavior of the response at different atomization temperatures, as the acid concentration is varied. As expected, the magnitude of the signal increases with the acid concentration and atomization temperature. However, as in Figure 6, there is a region where the signal changes slightly with the acid concentration.

Finally, the simultaneous variation of ashing and atomization temperatures was evaluated at an acid concentration of 2% v/v (−0.6 coded variable), as shown in Figure 8. Similar trends were observed in the response as the atomization temperature increases at different ashing temperatures. At a fixed atomization temperature, the signal is almost constant at low ashing temperatures. However, the peak area decreases markedly at high atomization temperatures as the ashing temperature is varied.

**Theoretical Calculations.** Previous calculations by Sierraalta et al.[26] for $Mo/C_{24}H_{12}$ (Mo/coronene) were carried out by taking into account the interaction of one molybdenum atom with different adsorption sites; see Figure 1. Adsorption on 6-fold, bridge, and on top sites were studied, optimizing Mo–coronene distances at different spin multiplicites. A triplet state was the most stable one in all cases. A summary of scaled binding energies (with respect to the dissociation energy of the Mo–C diatomic molecule) for the Mo–coronene system is presented in Table IV. The average values of equilibrium bond distances, charge, and adsorption energies for different adsorption sites (on top, bridge, and 6-fold on edges and in the center of the $C_{24}H_{12}$) reveal the following trend in adsorption energies: 6-fold > bridge > on top. With respect to the Mo–surface equilibrium bond distances, an expected trend is observed: a larger Mo–surface coordination implies a shorter Mo–surface distance. In addition, an electronic charge transfer from the surface to the Mo atom occurs in all cases.

On the basis of the experimental fact that, in the Mo atomization on a graphite surface, small grains of Mo may be formed,[27] this work is focused on the diffusion process of the Mo species on the modeled graphite surface. Here, the

(27) (a) Sturgeon, R. E.; Chakrabarti, C. L. *Anal. Chem.* **1977**, *49*, 90–97. (b) Chakrabarti, C. L.; Shaloe, W.; Marcantonio, F.; Headrick, K. L. *Spectrochim. Acta* **1986**, *41B*, 651–667.

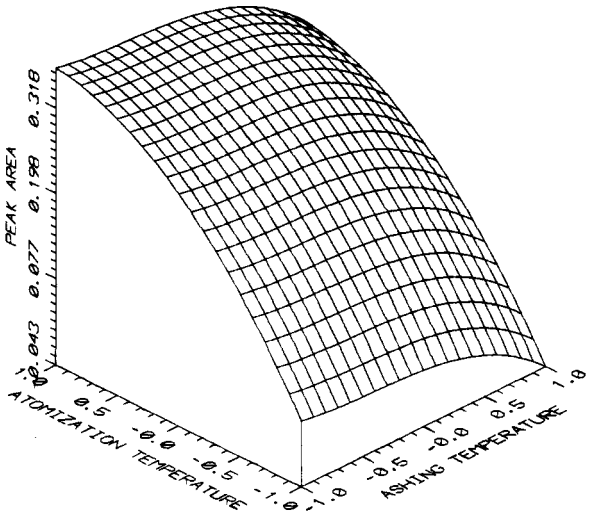


**Figure 8.** Surface response for atomization and ashing temperatures at the acid concentration of 2% v/v.

**Table IV. Adsorption Properties of the Molybdenum Atom Chemisorbed over a Modeled Graphite Surface**

| site | bond length (Å) | adsorption energy (kcal/mol) | charge on molybdenum (au) |
|---|---|---|---|
| 6-fold | 2.25 | −158.19 | −0.51 |
| bridge | 2.06 | −126.44 | −0.40 |
| on top | 1.97 | −120.50 | −0.41 |

**Table V. Orbital Occupancies, Bond Orders, Charges, and Diatomic Energies (DE) of the Mo Atom and $MoO_3$ Adsorbed on Sites I–III of the Coronene System**

| | orbital occupancy of the Mo atom | | | bond order (Mo–C) | | | total DE (Mo–C) |
|---|---|---|---|---|---|---|---|
| site | sp | d | total | sp–sp | sp–d | total | (au) |
| | | | Mo | | | | |
| I | 0.72 | 5.80 | 6.52 | 3.06 | 0.84 | 3.90 | −1.74 |
| II | 0.63 | 5.82 | 6.45 | 1.10 | 0.56 | 1.66 | −0.68 |
| III | 0.77 | 5.72 | 6.49 | 3.18 | 1.00 | 4.18 | −1.91 |
| | | | $MoO_3$ | | | | |
| I | 1.05 | 5.10 | 6.15 (−0.70)[a] | 2.64 | 0.63 | 3.27 | −1.43 |
| II | 1.02 | 5.07 | 6.09 (−0.58) | 1.02 | 0.34 | 1.36 | −0.55 |
| III | 1.08 | 5.13 | 6.21 (−0.64) | 2.80 | 0.77 | 3.57 | −1.57 |

[a] Values in parentheses are total charges on $MoO_3$.

diffusion process is considered through 6-fold and bridge sites, because these are the most stable sites for Mo adsorption. They are labeled I–III in Figure 1.

In order to understand the nature of the Mo–C bond, orbital occupancies, bond orders, and diatomic energies of Mo–C on these sites for the coronene/Mo and coronene/$MoO_3$ systems are listed in Table V. Oxidized molybdenum is included here because, at early stages of the thermal treatment, it has been proposed in the literature[27] as one of the most probable moieties. Comparison of the orbital occupancy of Mo on the surface with that of the Mo free atom in the ground state ($4d^5 5s^1$) reveals that a net electronic transfer from the coronene to d(Mo) orbitals occurs upon Mo chemisorption, in conjunction with a Mo(spd) hydridization. The population of the Mo atom in Mo/coronene is higher than in $MoO_3$/coronene, because the oxygen atoms withdraw electron density from Mo. Nevertheless, the total electronic transfer to $MoO_3$ (−0.70, −0.58, and −0.64) is larger than that to Mo (−0.52, −0.45, and −0.49) for sites I–III, respectively.

The total bond order values indicate that the Mo–C bonds are mainly for the sp–sp type with some important sp–d orbital

**Table VI. Orbital Occupancies, Bond Orders, Charges, and Diatomic Energies of the Mo Atom and $MoO_3$ Adsorbed on Sites I–III of the Coronene/$H^+$ System**

| | orbital occupancy of the Mo atom | | | bond order (Mo–C) | | | total DE (Mo–C) |
|---|---|---|---|---|---|---|---|
| site | sp | d | total | sp–sp | sp–d | total | (au) |
| | | | Mo | | | | |
| I | 0.67 | 5.32 | 6.00 | 3.00 | 0.96 | 3.96 | −1.73 |
| II | 0.60 | 5.59 | 6.19 | 1.10 | 0.60 | 1.70 | −0.71 |
| III | 0.70 | 5.54 | 6.22 | 2.81 | 0.87 | 3.68 | −1.65 |
| | | | $MoO_3$ | | | | |
| I | 1.08 | 5.14 | 6.22 (−0.69)[a] | 2.69 | 0.74 | 3.43 | −1.49 |
| II | 1.01 | 5.04 | 6.05 (−0.48) | 1.06 | 0.42 | 1.48 | −0.58 |
| III | 1.03 | 5.02 | 6.05 (−0.42) | 2.67 | 0.81 | 3.48 | −1.56 |

[a] Values in parentheses are total charges on $MoO_3$.

contributions. The orbitals on C atoms are mainly $p_Z$ with some contributions from s-orbitals. This small sp-hybridization allows a major overlapping between the orbitals of the Mo atom adsorbed in a 6-fold site and those of carbon atoms located at the aromatic ring. The bond orders and diatomic energies indicate that the 6-fold absorption site presents a stronger bond than the bridge one, in both cases (Mo/coronene and $MoO_3$/coronene). Obviously, in the case of $MoO_3$, the Mo–C bonds are weaker because the Mo atom shares part of its electronic density with three oxygen atoms. The greater stability of Mo on site III, with respect to site I, is due to the fact that Mo interactions with carbon edge atoms of coronene are stronger than those with the central atoms.

In order to model the experimentally observed effects of mineral acids in molybdenum atomization, the adsorption of Mo and $MoO_3$ was studied in the presence of a proton coadsorbed on sites IV or V over the model graphite surface (Figure 1). These sites were selected because previous calculations[26] indicate that adsorption of hydrogen occurs preferentially at edge atoms, although adsorption on central atoms is not discarded. The analysis of these theoretical results is focused on orbital occupancies, bond orders, charges, and diatomic energies of a molybdenum atom adsorbed on sites I–III of the Mo–$H^+$/coronene system, as shown in Table VI.

Similar trends in Mo/coronene and in $MoO_3$/coronene systems were found. A net charge transfer to Mo(d) orbitals is observed. However, since the proton charge is almost neutralized by the surface electrons, there is less electronic transfer from the surface to the Mo atom than in the nonprotonated case. The proton adsorption produces salient rearrangements in the adsorbate and surface charge distributions. Mo charges on sites I–III in Mo–$H^+$/coronene decrease 0.52, 0.36, and 0.27 au, respectively, with respect to the Mo/coronene case. For $MoO_3$, the charge changes are of minor magnitude, 0.01, 0.10, and 0.22 for sites I–III, respectively, because of the electronegativity of oxygen atoms in $MoO_3$. Bond orders and diatomic energies show a tendency to increase; i.e., Mo–C bonds in both adsorbates are strengthened, except in site III in which the adsorbates are directly or indirectly interacting with the $H^+$ atom. Note that the diffusion process from III → II → I when $H^+$ is present should be favored, because the bond strengths are higher on sites I and II and smaller on site III than in the case of the nonprotonated surface.

Potential energy curves for diffusion of Mo on the model carbon surface with and without protonation are shown in Figure 9. It is clear from these results that Mo diffusion on a nonprotonated surface from site III to site I and vice versa is very difficult because of the high energetic diffusion barrier. The coadsorption of $H^+$ lowers the diffusion barrier and

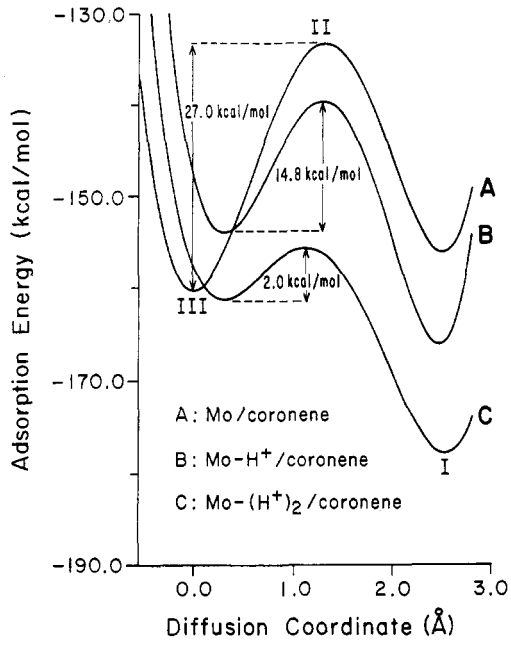


**Figure 9.** Potential energy curves for diffusion of a Mo atom on a modeled graphite surface with and without $H^+$ atoms coadsorbed.

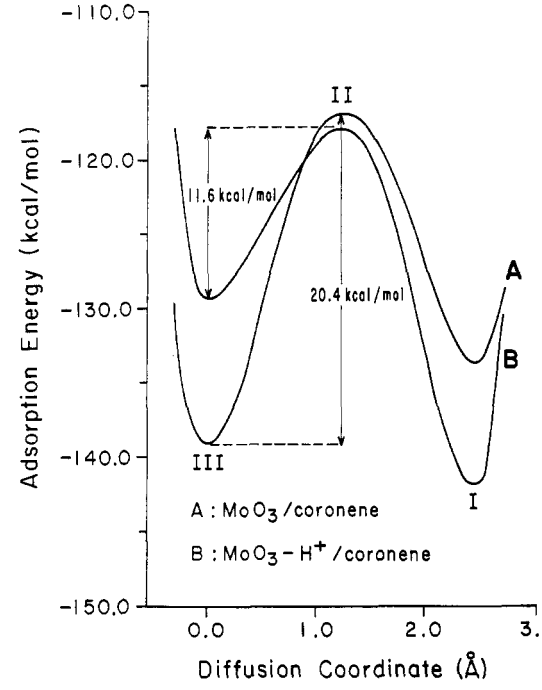


**Figure 10.** Potential energy curves for diffusion of the $MoO_3$ molecule on a modeled graphite surface with and without $H^+$ atom coadsorbed.

stabilizes adsorption on sites I and II, with respect to site III. The destabilization on site III may be due to a competition between the Mo atom and the proton for bonding to the carbon atom on site IV. Therefore, the charge driven from the surface by the $H^+$, and the formation of a relatively strong bond between the proton and the surface, lower the diffusion barrier from site III to site I. Thus, the diffusion barrier decreases from above 27 kcal/mol in Mo/coronene to 15 kcal/mol in the Mo–$H^+$/coronene system. A more drastic decrease is observed when a second proton is coadsorbed over site V (see Figure 1). The diffusion barrier is lowered to a value of 2 kcal/mol.

In the case of $MoO_3$, the situation is quite similar. The diffusion barrier of $MoO_3$ in going from site III to site I decreases from about 20 kcal/mol in coronene to 12 kcal/mol in the Mo–$H^+$/coronene system.

**Interpretation of Experimental and Theoretical Results.** In this section, experimental and theoretical results are analyzed in terms of the interaction of Mo species with the graphite tube surface. Figure 3 clearly indicates that mineral acids enhance the Mo eaaas signal. One unanswered question is how do acids affect the Mo atomization? Two possible mechanisms may influence the enhancement of the Mo signal: first, in some way acids help to remove Mo species chemisorbed on the surface or in bulk; second, acids avoid the loss of molybdenum by volatilization at the ashing stage. The analysis of the results given in Figure 4a shows (a) part of the Mo in each run is retained in some adsorption sites on the graphite and (b) mineral acids ($HNO_3$ and HCl) facilitates the removal of Mo from the surface at the atomization state, as is confirmed by Figure 4b,c. With respect to the molybdenum loss, the presence of acid does not seem to prevent the decrease in the absorbance curve due to volatilization; see Figure 6.

Because at atomization temperatures the acid concentration on graphite would be negligible, one may conclude that the main function of acids is to facilitate, at early stages of the heating program, the formation of Mo species that can be easily atomized. Mendoza and Ruette[25] found that hydrogen chemisorption on model graphite platelets is stronger on the edge atoms (1.95 eV) of the platelets than on the central atoms (0.60 eV). In addition, the energetically most favorable coverage is obtained if the hydrogens are adsorbed on both sides of these platelets, suggesting the possibility of intercalated hydrogen atoms on the graphite bulk at relatively high temperatures. Therefore, it is expected that at the beginning of the heating program the $H^+$ concentration on the graphite surface would be sufficient to allow reorganization of the Mo species strongly chemisorbed on or trapped in the graphite bulk.

According to our theoretical results, $H^+$ and Mo adsorptions preferentially occur at on top and 6-fold center sites located at the edges of the modeled graphite surface (sites IV and V, and III in Figure 1), respectively. The presence of $H^+$ lowers the diffusion barrier (Figures 9 and 10) of the Mo species, facilitating movement from the edge to center sites on the graphite platelets. Thus, the effect of the protons is to agglomerate the Mo species in the center of small graphite planes (pyrolitic graphite), in such a way that the atomization efficiency is improved.

Experimental response curves at constant ashing temperatures, with varying acid concentration, display three regions (A–C) shown in Figure 6, two (A, C) in which the increase of the acid concentration enhances the Mo aa signal and one (B) where the change of acid concentration almost does not affect the Mo signal. This result may be interpreted as due to the presence of at least two types of chemisorbed species on the graphite tube, one that appears in the region of low acid concentration (A) and the other at high concentration (C). According to our calculations for diffusion of Mo species (see Figures 9 and 10) in region C, the Mo chemisorbed species will require greater acid concentration to migrate on the graphite surface.

There is some experimental evidence that atomization of Mo takes places through two possible mechanisms:[16] sublimation of Mo(s) to Mo(g) and dissociation of MoC(g). The formation of the Mo(s) phase is due to association of Mo species which may be facilitated by the coadsorption of $H^+$, as shown above. In the case of oxidized species, it is well-known that in an acid medium, these tend to condense and form several types of polymolybdate ions.[28] One can not then discard the formation of polymolybdates in liquid phase, even though the Mo concentration is too low. Nevertheless, because

(28) Cotton, F. A.; Wilkinson, G. *Advanced Inorganic Chemistry*, 3rd ed.; Interscience Publishers: New York, 1972; p 951.

condensation, adsorption, and diffusion are processes in equilibrium, the association of Mo species may occur both in the liquid phase and on the surface.

Finally, note that the theoretical part of this work is not in any manner conclusive, because our calculations were performed at a qualitative level. This is an on-going project where more experimental and theortical work has to be done in order to take into account, for example, the effect of Mo concentration in the multivariable optimization approach[29] and more complex surface models that consider adsorption on dislocations, ledges, arm-chair positions, interstitial Mo adsorption, and Mo–Mo interactions. In order to attain a more complete and feasible surface model two or three platelets modeled by coronenes[30] or pyrenes have to be included. In addition, surface relaxation[31] due to Mo chemisorption must be considered.

## CONCLUSIONS

(a) The presence of mineral acids enhances the Mo eaaas signal because it favors the formation of associated Mo species that can be more easily atomized. Memory effects were confirmed by the release of some Mo species tightly chemisorbed on the graphite tube when an acidified solution was used as a blank.

(b) The adsorption of $MoO_3$ and Mo occurs preferently on 6-fold center sites located at the edges, with electronic transfer from the graphite to the Mo adsorbate. Theoretical calculations showed that the nature of the Mo–C bond is mainly of sp–sp type, with an important contribution of sp–d orbital interaction.

(c) Experimental results using a multivariable optimization approach suggest that at least two Mo species are formed as the acid concentration is increased; one at low concentration and another above 6% v/v HCl.

(d) Theoretical calculations for potential energy curves of adsorbed Mo and $MoO_3$ on a modeled graphite surface showed that acids ($H^+$) decrease the diffusion barriers for migration of Mo chemisorbed species. This result is interpreted as an indication of the formation of Mo-aggregated species in the graphite surface by thermal and acid treatment.

## ACKNOWLEDGMENT

The authors gratefully acknowledge CONICIT for partial financial support and EMSCA Co. for allowing us the use of a SUN Sparc workstation.

RECEIVED for review September 24, 1992. Accepted January 2, 1993.

(29) Araujo, P. W.; Gomez, M. J.; Benzo, de Z. A.; Castillo, C. *Chemom. Intell. Lab. Syst.* **1992**, *16*, 203– 211.

(30) Rodriguez, J.; Sánchez-Marin, J.; Torrens, F.; Ruette, F. *J. Mol. Struct.* **1992**, *254*, 429–441.

(31) Fromherz, T.; Mendoza, C.; Ruette, F. *Mon. Not. R. Astron. Soc.*, in press.